Seventh Symposium on Salt, Vol. I 67–74 (1993)
Elsevier Science Publishers B.V., Amsterdam

Slow Experimental Deformation of Avery Island Salt

S.T. Horseman*, J.E. Russell, J. Handin, and N.L. Carter

Center for Tectonophysics, Texas A&M University, College Station, TX 77843, USA

ABSTRACT

Two 100 mm diameter by 200 mm long cylinders of Avery Island (A.I.) rocksalt have been subjected to a constant strain rate of 10^{-9} s^{-1} at 15 MPa confining pressure and 50 and 100°C. The experimental conditions have been virtually constant over a period of about 3.5 years during which the samples have shortened homogeneously by about 11%. The specimen deformed at 100°C (Test 47) reached a steady-state stress of 4.7 MPa at 2% strain whereas that at 50°C (Test 46), still slightly work-hardening, reached a quasi steady-state stress level of 12.6 MPa. Microstructural analysis reveals that dislocation glide and cross-slip dominated deformation at 50°C whereas, at 100°C, subgrain development is excellent indicating extensive dislocation climb.

These data points from Tests 46 and 47 were combined with nine earlier constant strain rate steady-state test results to provide, by nonlinear least squares, the relation

$$\dot{\varepsilon}_s = 6.5 \times 10^{-5} \exp(-69.7/RT\ 10^{-3})\sigma^{5.9} \quad (1)$$

When added to 27 A.I. constant stress test data points of RE/SPEC Inc., ten of the low stress, low strain rate tests at 100 and 200°C are very well fit by $\dot{\varepsilon} \alpha \sigma^{3.4}$ whereas the remaining high strain rate, high stress quasi steady-state data are well fit by $\dot{\varepsilon} \alpha \sigma^{5.2}$. This change in behavior, which must result from a change in dominant, rate-limiting, mechanism bears importantly on inferences concerning rates of natural salt deformation. At comparable temperature and stress, the $\varepsilon \alpha \sigma^{3.4}$ relation predicts strain rates two orders of magnitude higher than does the $\dot{\varepsilon} \alpha \sigma^{5.2}$ equation; the latter is likely to be most pertinent to geotechnical engineering applications.

INTRODUCTION

An increasing awareness that rocksalt is an accessible natural medium of enormous geotechnical importance has emphasized the need for a fundamental understanding of its flow properties and processes. That rocksalt is impervious and flows readily in the long term but is as strong as ordinary concrete in the short term, makes this material ideal for providing barriers to hydrocarbon migration and for development of underground mines. However, for predictions of, for example, mine or cavern closure rates or the rate of salt diapir intrusion, creep flow laws for the salt (at least) must be known. By far the most thoroughly studied rocksalt to date has been Avery Island domal salt. To that data base, we add two very unusual experiments carried out in compression at a constant strain rate of 10^{-9} s^{-1} at 15 MPa confining pressure and at temperatures of 50 and 100°C, both over a ca. 3.5 year time span to ca. 11% natural strain. These experiments have provided new insight on rocksalt flow behavior.

APPARATUS

The experimental apparatus used has been described in detail in Horseman and Handin (1990) and only a summary is given here. Each of the two identical testing machines consists essentially of a screw-driven 100-ton (0.9 MN) press that axially loads a jacketed, cylindrical specimen in a triaxial cell. The 100 by 200-mm specimen is placed between Lucalox spacers, this assembly being jacketed using 2.5 mm thick seamless sleeves of molded Viton, secured with hose clamps. The triaxial cell into which the sample assembly is placed is heated externally with temperature measured by sensors mounted on the jacket at the center and opposite sides of the specimen. A third sensor, that provides the temperature control signal, is mounted outside the cell. Con-

* Now at Intera Information Technologies Ltd., 14B Burton St., Melton Mowbray, Leics. LE13 1AE, UK

fining pressure is provided by mineral oil pressurized by a Sprague 10,000 psi (70 MPa) air-driven pump, through a large, floating-piston separator. Total force on the loading piston is measured by a 100,000 pound (0.445 MN) Strainsert Model FL100C(C) load cell. Displacement of the lower moving plate with respect to the upper stationary plate is measured by a Schaevitz Model 200-HR LVDT. Analog output from all transducers is fed to a Yew, model 3081, 30-channel hybrid A to D strip-chart recorder.

Specimen 46 was brought to pressure (15 MPa) and temperature (50°C), and loading began at 10^{-9} s^{-1} on April 21, 1988, and ended on October 14, 1991. Similarly, loading on specimen 47 (15 MPa, 100°C) began on May 4, 1988 and ended on October 7, 1991. Apart from a few power failures, both experiments were remarkably stable and leak-free during the entire 3.5 year period. Temperature varied little throughout as a back-up power supply (battery array) activated and supplied the required power during each power failure. Following Horseman and Handin (1990), the force is believed to be accurate to ±200 pounds (890 N), confining pressure to ±5 psi (34 KPa) and temperature to 1.5°C. Displacement rate (synchronous DC motor driving the transmission and frictionless screw) is held constant to ±1% and strain rate varies by 10% for a specimen shortened by a factor of 0.1.

STARTING MATERIAL

Avery Island domal salt is the purest, most homogeneous salt yet discovered (Hansen and Carter, 1984; Handin et al., 1986; Horseman and Handin, 1990). This material is unusually fine-grained and virtually free of anhydrite and negative crystals both within the halite crystals and along grain boundaries. The content of any foreign ion is less than 100 ppm, *in situ* water content is less than 50 ppm, porosity is less than 0.5% and permeability to nitrogen is as low as 10^{-21} m^2. There is a weak preferred orientation of a-axes normal to the long axes of cores (vertical in nature).

The specific material used for tests 46 and 47 (designated site D by Horseman and Handin, 1990) was collected in 1985 from the 500-foot (150 m) level of the mine but 60 m distant from sites A, B and C (Handin et al., 1986). Specimens prepared and shipped by RE/SPEC Inc. are in the form of right circular cylinders, 100 mm in diameter by 200 mm long, protected by Saran Wrap, then aluminum foil with an outer sleeve of wax. The as-received AI/85 or site D batch is composed of clear interlocking halite crystals with the grain size ranging from 2 to 13 mm and averaging about 7.5 mm. Each halite crystal, cleaved and etched, contains subgrains having an average diameter of 0.21 mm within which the free dislocation density is estimated to be about 10^7 cm^{-2}.

EXPERIMENTALLY DEFORMED SPECIMENS

Macroscopic features

Figure 1 shows the two experimentally deformed specimens separated by an undeformed specimen of the AI/85 or D batch. Except for the ends of the specimens, deformation has been quite homogeneous as revealed by four sets of diametral measurements at five equally spaced locations along the axial surface (see markings on AI47, Fig. 1, right). The weight of each specimen was lower by 2.4 g (0.07%) than the initial weight (ca. 3500 g) but it is not certain that the same scale was used. Therefore the weight loss is suspect; the density, =2.17, apparently has remained essentially unchanged (calculations assume homogeneous strain).

In order to characterize the samples more completely prior to cutting, they were translated through a Technicare Delta 100, 120 KV, X-ray Cat Scanner having a 7 mm slice thickness, 1 mm in-plane resolution and 2 min scan time. No substantive differences are observed in the CT (computer tomography) images either between undeformed and deformed samples or along the core axis of the deformed specimens. These observations also attest to the homogeneity both of the material and of deformation.

Microscopic features

Specimens 46 and 47 were next sawn into two half cylinders (normal to the core axis); one half of each has been preserved. A 1-inch disc was then cut from the central portion of the remaining half and the disc was cut into quarters. Thin sections were prepared from one quarter segment from each specimen. No cracks or photoelastic effect are present. Grain boundary migration may have occurred, more so for the 100°C test than for the 50°C one.

Cleavage chips parallel to {100}, obtained from the undeformed material and two test specimens, were immersed for 30 s in a solution of 4 g $FeCl_3$/liter of glacial acetic acid (Mendelson, 1961), rinsed quickly in absolute ethyl alcohol and then anhydrous ether. The resulting substructure, revealed by preferential etching along dislocation lines, is as shown in Fig. 2. Figure 2A shows the substructure of the AI/85 starting material; the dark, irregular boundaries enclosing regions of rather high dislocation (pit) density are boundaries of subgrains having an average diameter of 208 μm. Figure 2B shows the substruc-

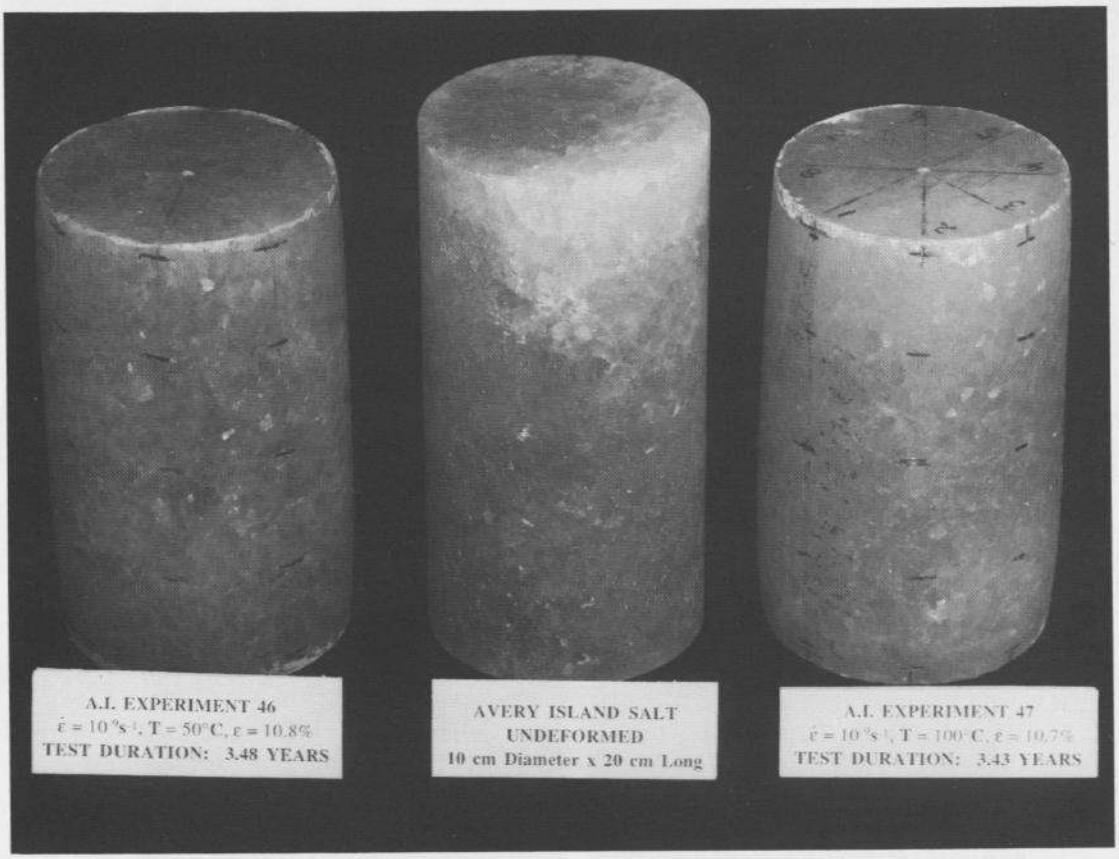

Fig. 1. Photograph of the experimentally deformed specimens flanking a 10 cm-diameter x 20 cm-long undeformed one.

ture of specimen 46 (50°C; 10^{-9} s^{-1}); the NE-trending linear features are cleavage steps, to be ignored. The very high dislocation density and wavy slip bands (NS-trending bands) are typical of substructural development limited by the cross-slip of screw dislocations; no subgrains have formed in this specimen.

In contrast, well-developed subgrains, having an average diameter of 28 μm, enclosing regions of low dislocation density, characterize specimen 47 (100°C, 10^{-9}; Fig. 2C). In addition to the cross-slip of screw dislocation segments, well-formed subgrains require extensive climb of edge dislocations by atom or vacancy diffusion and this process is generally considered to control the creep rate during development of this type of substructure. At this scale, the deformation is not so homogeneous as is revealed by the substructure shown in Fig. 2D. In that photomicrograph the substructure typical of specimen 47 (lower right) grades into a zone (upper left) in which the subgrain size is smaller and the dislocation density is higher. There is as yet no clear explanation for these localized 'disturbed' zones either from the strip chart record or from the material; we merely note their occurrence.

Mechanical response

Applying suitable corrections, the force-displacement data recorded during a constant strain rate experiment are reduced to stress–strain curves, for a given temperature and pressure. In Fig. 3, we plot true differential stress (axial differential force divided by instantaneous cross-sectional area of the specimen assuming homogeneous, isovolumetric deformation) against natural (logarithmic) strain (determined from externally measured displacements corrected for machine stiffness). Following Horseman and Handin (1990), we estimate the absolute accuracy of corrected stress–strain values to be ±3–4% with the relative accuracy being somewhat better. The solid curves are those determined for tests 46 and 47 and the dashed curves included for comparison (Horseman and Handin, 1990) are for tests at a rate one decade higher. The stress–strain curve for Test 47 shows that steady-state flow was achieved at 2% strain and remained at a constant value of flow stress, 4.7 MPa, thereafter. All other curves show slight work-hardening at the highest strains and the material may be described as being in quasi steady-state flow. Note that a 50°C increase in temperature reduces the flow stress by about 8

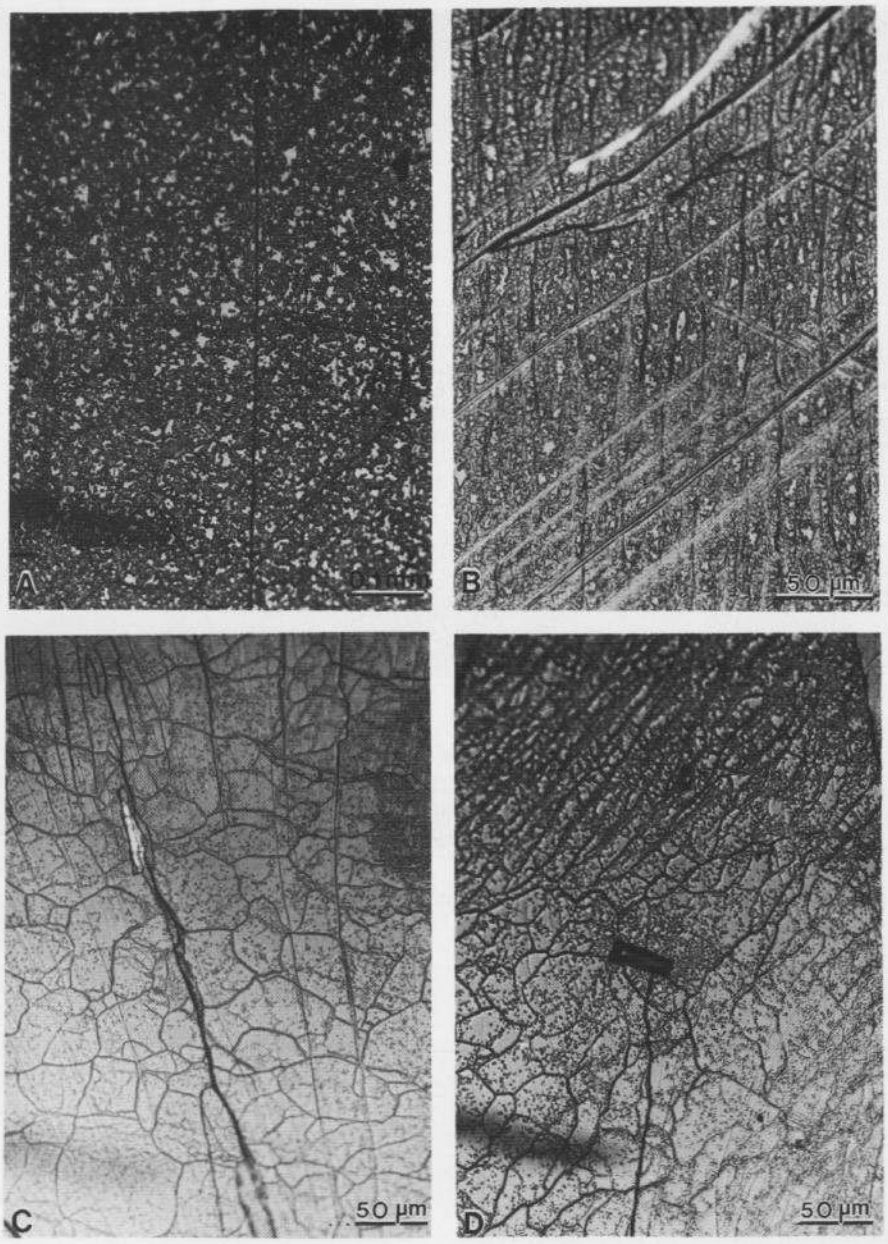

Fig. 2. Photomicrographs of etched cleavage fragments from undeformed AI/85 or site D salt (A), 50°C specimen 46 (B), and 100°C specimen 47 (C,D). See text for discussion.

MPa whereas a ten-fold decrease in strain rate reduces it by about 5 MPa.

The flow stresses at 10% strain for tests 46 and 47 are plotted in log stress versus log strain rate space in Fig. 4, along with the results of nine earlier constant strain rate tests (Table 1) on A.I. salt (Horseman and Handin, 1990). Of these prior quasi steady-state experiments, five are tests on site D salt and four were carried out on AI salt from sites C and B, the strongest two of the four sites tested earlier (Handin et al., 1986) with strengths comparable to material from site D (Horseman and Handin, 1990).

The 11 data points shown were fit by non-linear, least squares regression to the well-known power law (e.g., Weertman and Weertman, 1970)

$$\dot{\varepsilon}_s = A \exp(-Q_s/RT)\sigma^n \quad (1)$$

where the coefficient A (MPa^{-n} s^{-1}) is a slightly temperature sensitive material parameter, Q_s is the apparent activation energy for flow (J/mole) limited by the dominant mechanism, R is the universal gas constant (8.314 J/mole K), T is absolute temperature, σ is the flow stress and n, the stress exponent.

TABLE 1

Avery Island rocksalt. Constant strain rate test data

Temp. T(°C)	Strain rate (s^{-1}) $\dot{\varepsilon}(s^{-1})$	Stress (10% ε) ($\sigma_1-\sigma_3$, MPa	Confining pressure P_c (MPa)	Subgrain size (μm)*	Measurements No.	Test I.D.	Source**
50	10^{-8}	16.4	15.0	—	—	36D	H&H
50	10^{-9}	12.3	15.0	—	—	46D	This study
75	10^{-7}	17.9	15.0	—	—	33D	H&H
100	10^{-6}	18.9	15.0	6.8	151	35D	H&H; R et al.
100	10^{-7}	14.1	15.0	8.8	178	34D	H&H; R et al.
100	10^{-7}	15.6	3.4	—	—	45C	H&H
100	10^{-8}	9.3	15.0	13.8	215	42D	H et al.; R et al.
100	10^{-9}	4.7	15.0	28.0	501	47D	This study
150	10^{-6}	11.7	3.4	10.3	230	20B	H et al.; R et al.
200	10^{-6}	8.6	3.4	17.3	192	9C	H et al.; R et al.
200	10^{-7}	6.8	3.4	21.5	173	43C	H&H; R et al.

*Avery Island AI/85/32/12/2-3/1 undeformed (site D); average subgrain diameter is 208 μm.
**H et al. = Handin et al., 1986. H&H = Horseman and Handin, 1990. R et al. = Russell et al., 1990.

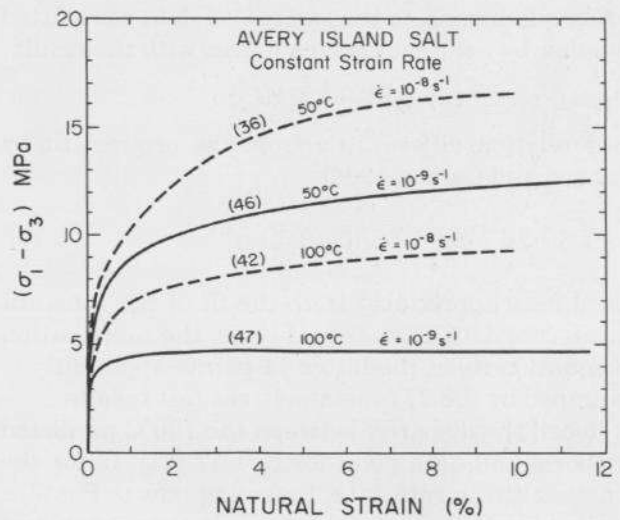

Fig. 3. Stress–strain curves (solid) for tests 46 and 47 compared with curves (dashed) for experiments at comparable temperature but at $\dot{\varepsilon} = 10^{-8}\ s^{-1}$ (Horseman and Handin, 1990).

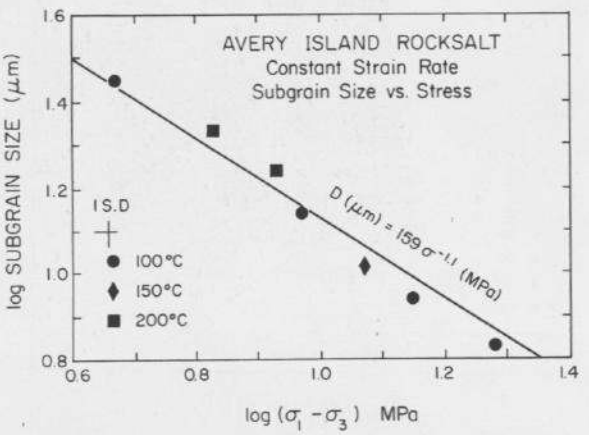

Fig. 4. Log stress vs. log subgrain size plot of constant strain rate results listed in Table 1.

The corresponding relation obtained for our constant strain rate quasi steady-state data at 10% strain is

$$\varepsilon_s = 6.5 \times 10^{-5} \exp(-69.0/RT\ 10^{-3})\sigma^{5.9} \qquad (2)$$

We point out here, and discuss later, that while test point 46 (Fig. 4) lies very near the 50°C isotherm predicted from equation (2), test point 47 falls about 3 MPa below the 100°C isotherm.

Inferences concerning steady-state flow stress levels in natural salt deformation have come from calibrations of average diameters of subgrains formed during steady-state flow in laboratory experiments (Carter et al., 1982; Carter and Hansen, 1983; Handin et al., 1986; Russell et al., 1990). Inasmuch as observations on many materials (e.g., Takeuchi and Argon, 1976) are consistent with subgrain size being an inverse function of stress only, careful calibration of this the paleopiezometer for halite is important. Pertinent data for seven specimens listed in Table 1 are plotted in log s vs. log subgrain size space in Fig. 4. A least squares fit to these data yields

$$D(\mu m) = 159\ \sigma^{1.1} \qquad (3)$$

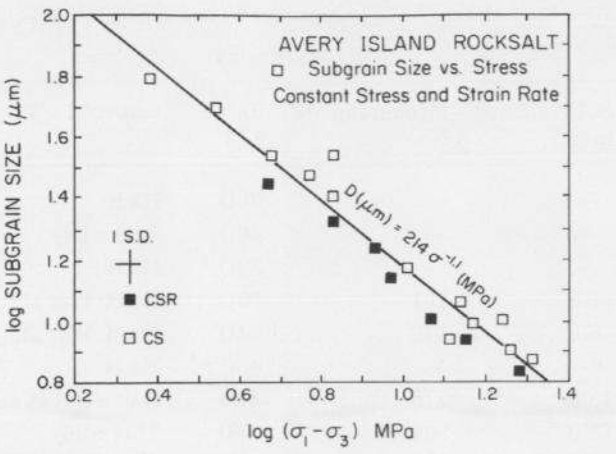

Fig. 5. Log stress vs. log subgrain size plot for combined constant stress and constant strain rate quasi steady-state data for Avery Island rocksalt.

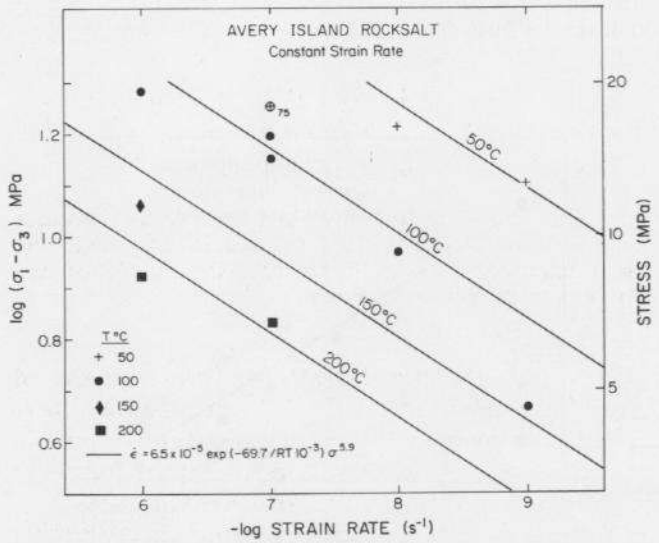

Fig. 6. Log stress vs. log strain rate plot of all quasi steady state (at 10% strain) constant strain rate data for Avery Island salt. Isotherms are plotted on the basis of a nonlinear least squares fit to the data (lower left and equation (2) in text).

DISCUSSION AND CONCLUSIONS

We now consider our constant strain rate test results in comparison with the more extensive constant stress (creep) test results on Avery Island rocksalt obtained primarily by scientists at RE/SPEC Inc. For convenience, we first analyze the subgrain size–stress relation using our 7 data points and 14 of 16 of the creep tests employed for that purpose by Carter et al. (1982); two tests were deleted because only 24 measurements were made for one (AI-4B-4J) and the material used for the other (W9-2668) is unidentified. The combined data are presented in Fig. 5 where they are fit by linear least squares to

$$D(\mu m) = 214\ \sigma^{1.1}\ (MPa) \quad (4)$$

This empirical relation should be substituted for the initial relation (Carter et al., 1982)

$$D(\mu m) = 190\ \sigma^{1.0} \quad (5)$$

for paleopiezometric considerations, although differences in flow stress estimates for natural salt deformation are only about 0.1 MPa.

Next, we combine our 11 test results with 27 constant stress test results on the same material (Hansen and Carter, 1984; Senseny, 1988) to assess any obvious effects of load path on the steady-state stress levels. Figure 7 shows the combined data plotted in -log strain rate vs. log stress space; a careful perusal of relative locations of constant stress data points (open symbols) with respect to the constant strain rate ones (solid) indicates that, at comparable conditions, steady-state stress for the latter are generally slightly lower than for the former. The difference is small, however, and may not be significant, so the two sets of data were fitted together by nonlinear least squares with the result

$$\dot{\varepsilon}_s = 2.0 \times 10^{-4} \exp(-62.3/RT\ 10^{-3})\sigma^{4.5} \quad (6)$$

This relation differs little from the original fit by Hansen and Carter, 1984)

$$\dot{\varepsilon} = 7.6 \times 10^{-4} \exp(-66/RT\ 10^{-3})\ \sigma^{4.5} \quad (7)$$

but differs appreciably from the fit of the constant strain rate data alone (equation 2); the contribution to equation (6) of the latter 11 points apparently is swamped by the 27 constant stress test results.

Recall the disparity between the 100°C predicted isotherm and data point for test 47 (Fig. 6) for the constant strain rate data. Referring now to Fig. 7, a similar disparity occurs as regards that point, two 100°C constant stress data points immediately above it and the 200°C constant stress data point at a strain rate of $3.4 \times 10^{-9}\ s^{-1}$. These deviations suggest to us that there may be a change in behavior at low stresses and strain rates, perhaps associated with a change in the rate-controlling deformation mechanism. Accordingly, we refit the five data points at 100°C and $\dot{\varepsilon} \leq 10^{-8}\ s^{-1}$ and five 200°C data points at $\dot{\varepsilon} \leq 10^{-7}\ s^{-1}$, in the same manner as before, with the result

$$\dot{\varepsilon} = 8.1 \times 10^{-5} \exp(-51.6/RT\ 10^{-3})\ \sigma^{3.4} \quad (8)$$

The fit to the remaining data yields

$$\dot{\varepsilon} = 1.3 \times 10^{-4} \exp(-66.4/RT\ 10^{-3})\ \sigma^{5.2} \quad (9)$$

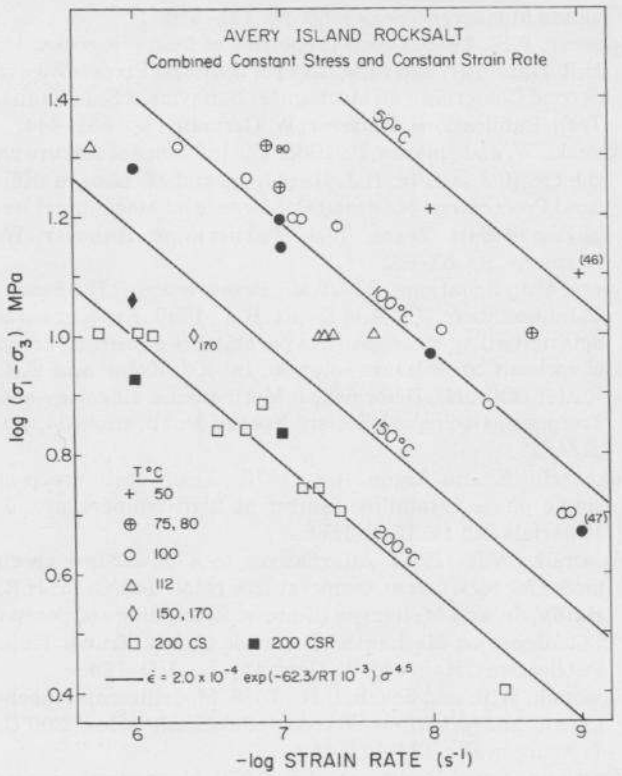

Fig. 7. Log stress vs. -log strain rate plot of combined quasi steady state constant strain rate (solid symbols) and constant stress (open symbols) test data. Isotherms are plotted on the basis of a nonlinear, least squares fit to the data as given by equation (6) in text and in lower left of the diagram.

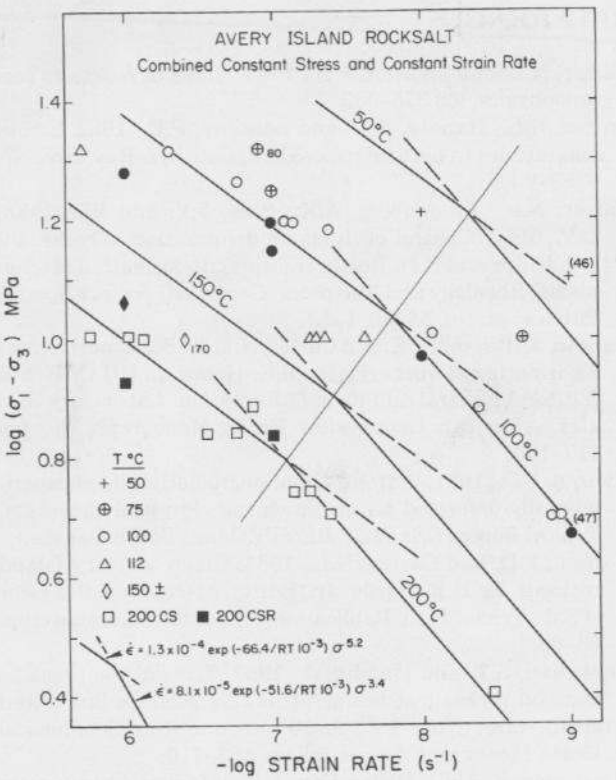

Fig. 8. Same data as Fig. 7 but fit by nonlinear, least squares to high-stress/high-strain rate data (equation (9) in text) and low-stress/low-strain rate data (equation (8) in text). See relations at lower left of the diagram.

Isotherms predicted from equations (8) and (9) are as shown in Fig. 8; it is evident that the low stress–low strain rate data are much better fit by equation (8) than by equation (6); (Fig. 7). The change in behavior to $\dot{\varepsilon} \alpha \sigma^{3.4}$ has not occurred in test 46 at 50°, 10^{-9} s^{-1}. Therefore, the boundary separating flow regimes must be deflected to the right at temperatures lower than 100°C and strain rates lower than 10^{-9} s^{-1}.

The change in behavior of the salt at low stresses and strain rates must have resulted from a change in the rate-controlling mechanism, perhaps, from cross-slip (Wawersik and Zeuch, 1986; Wawersik, 1988; Skrotski and Haasen, 1988) to climb of dislocations, although the lower apparent activation energy for the low-stress low-strain rate mechanism is not yet understood. Nevertheless, the change in behavior has highly significant implications as regards rates of flow of natural rocksalt. Strain rates predicted by the low stress, low strain rate relation (8) are about two orders of magnitude higher than are those predicted by the high strain rate-high stress equation (9). For example, at a temperature of 75°C, and a stress difference of 1 MPa (near the average stress for natural rocksalt deformation as deduced from subgrain size) the strain rate predicted by equation (9) is about 10^{-14} s^{-1} whereas that predicted by (8) is near 10^{-12} s^{-1}. The latter behavior is applicable to large-scale salt tectonics; the former is pertinent to geotechnical engineering concerns.

We conclude by pointing out that these results pertain to very dry rocksalt which we believe may represent the bulk of natural rocksalt deformational behavior. Should appreciable quantities of water be available, the behavior is quite different (e.g., Spiers et al., 1990) as are predictions of strain rates at various temperatures and flow stresses (Spiers et al., 1990; Carter et al., 1990).

ACKNOWLEDGMENTS

This research was partially supported by DOE/BES Award DE-FG05-87ER1371 and by NATO Grant CRG 900591. Special thanks go to J. Magouirk for his essential efforts during the entire test program. B. Turk also helped in this way. T. Orsi and a grant from the Petroleum Engineering Imaging Center provided CT images. Research discussions with A. Kronenberg and C. Spiers throughout this project have been very helpful.

REFERENCES

Carter, N.L. and Hansen, F.D., 1983. Creep of rocksalt. Tectonophysics, 92: 275–333.

Carter, N.L., Handin, F.D. and Senseny, P.E., 1982. Stress magnitudes in natural rock salt. J. Geophys. Research, 87: 9289–9300.

Carter, N.L., Kronenberg, A.K., Ross, J.V. and Wiltschko, D.V., 1990. Control of fluids on deformation of rocks. In: R.J. Knipe and E.H. Rutter (Editors), Deformation Mechanisms, Rheology and Tectonics. Geological Society Special Publication No. 54, pp. 1–13.

Handin, J., Russell, J.E. and Carter, N.L., 1986. Experimental deformation of rocksalt. In: B.E. Hobbs and H.C. Heard (Editors) Mineral and Rock Deformation: Laboratory Studies. American Geophysical Union Monograph, 36, pp. 117–160.

Hansen, F.D., 1987. Petrology, and micromechanics of experimentally deformed natural rock salt. Physical Processes, Topical Report RSI-0262, RE/SPEC Inc., South Dakota.

Hansen, F.D. and Carter, N.L., 1984. Creep of Avery Island rocksalt. In: H.R. Hardy, Jr., Editor, Mechanical Behavior of Salt, Trans. Tech. Publications, Clausthal, Germany, pp. 53–69.

Horseman, S.T. and Handin, J., 1990. Triaxial-compression tests on rocksalt at temperatures from 50° to 200°C and strain rates from 10^{-4} to 10^{-9}/s. American Geophysical Union Monograph Series, 56. pp. 103–110.

Mendelson, S., 1961. Dislocation etch pit formation in sodium chloride. J. Appl. Phys. 32: 1579–1583.

Russell, J.E., Carter, N.L. and Walker, S.C., 1990. A material model for Avery Island Rocksalt. American Geophysical Union Monograph Series, 56. pp. 111–118.

Senseny, P.E., 1988. Creep properties of four salt rocks. In: H.R. Hardy, Jr. and M.M. Langes (Editors) Proceedings of Second Conference on Mechanical Behavior of Salt. Trans. Tech. Publications, Hanover, W. Germany. pp. 431–444.

Skrotski, W. and Haasen, P., 1988. The influence of texture on the creep of salt. In: H.J. Hardy, Jr. and M. Langes (Editors) Proceedings of Second Conference on Mechanical Behavior of Salt. Trans. Tech. Publications, Hanover, W. Germany. pp. 83–88.

Spiers, C.J., Schutjens, P.M.T.M., Brzasowsky, R.H., Peach, C.J. Liezenberg, J.L. and Zwart, H.J., 1990. Experimental determination of constitutive parameters governing creep of rocksalt by pressure solution. In: R.J. Knipe and E.H. Rutter (Editors), Deformation Mechanisms, Rheology and Tectonics, Geological Society Special Publication 54, pp. 215–227.

Takeuechi, S. and Argon, A.S., 1976. Steady-state creep of single phase crystalline matter at high temperature. J. Materials Sci. 11: 1542–1566.

Wawersik, W.R., 1988. Alternatives to a power-law creep model for rock salt at temperatures below 160°C. In: H.R. Hardy, Jr. and M. Langes (Editors) Proceedings of Second Conference on Mechanical Behavior of Salt. Trans. Tech. Publications, Hanover, W. Germany. pp. 103–128.

Wawersik, W.R. and Zeuch, D.H., 1986. Modelling and mechanistic interpretation of creep of rocksalt below 200°C. Tectonophysics, 121: 125–152.

Weertman, J. and Weertman, J.R., 1970. Mechanical properties, strongly temperature dependent. In: R.W. Cahn (Editor), Physical Metallurgy, Elsevier, New York. pp. 983–1010.